ACS APPLIED POLYMER MATERIALS

Article

Cite This: *ACS Appl. Polym. Mater.* 2019, 1, 2731−2740

pubs.acs.org/acsapm

High Production Rate of High Purity, High Fidelity Nafion Nanofibers via Needleless Electrospinning

Monica Hwang, Muizz O. Karenson, and Yossef A. Elabd*

Department of Chemical Engineering, Texas A&M University, College Station, Texas 77843, United States

Supporting Information

ABSTRACT: This study demonstrates the needleless electrospinning of Nafion nanofibers via foam electrospinning. Compared to needle electrospinning, a 2 orders of magnitude higher production rate (9729 vs 14 mg h^{-1} m^{-2}) was obtained at similar fidelity (233 ± 62 vs 216 ± 69 nm fiber diameters). Additionally, needleless electrospinning produced defect-free high purity Nafion nanofibers (98 wt % Nafion) compared to no fibers (beads) using needle electrospinning at a similar polymer solution concentration. Furthermore, the Young's modulus and proton conductivity of the fiber mats produced by needleless electrospinning (42.6 MPa and 43.8 mS cm^{-1}, respectively) were higher than those produced by needle electrospinning (20.9 MPa and 18.0 mS cm^{-1}, respectively). Therefore, high fidelity, high purity Nafion nanofibers at higher production rates with improved mechanical properties and proton conductivity were produced with this needleless electrospinning technique.

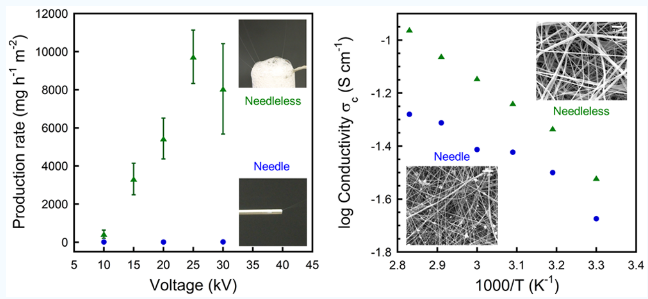

KEYWORDS: *Nafion, nanofiber, electrospinning, conductivity, ionomer, fuel cell*

1. INTRODUCTION

Nafion is a perfluorinated anionic (sulfonic acid) polymer that possesses excellent thermal, mechanical, and chemical stability, along with high water-saturated proton conductivity (ca. 0.1 S cm^{-1}), and therefore has been explored in various applications, including in chloralkali electrolyzers,[1,2] in sensors,[3−5] as superacid catalysts,[6−8] and most notably as a polymer electrolyte membrane and ionomer in hydrogen fuel cells.[9−13] Nafion is commercially available in several forms, including extruded and solution cast films, dispersions in aqueous alcohol solvents, and pellets. In addition to these forms, Nafion in nanofiber form has been reported and has shown to possess enhanced properties (e.g., proton conductivity) and subsequently enhances device performance.[14−38] One example includes the Snyder and Elabd[34] report on Nafion nanofibers that naturally form in fuel cell electrodes due to the heat (above Nafion's thermal transition) and pressure (tensile stress) of the fuel cell, which promotes the formation of Nafion nanofibers and subsequently improves fuel cell performance. Another example includes the Dong et al.[31] report on the super proton conductivity (>1 S cm^{-1}) of a single high purity Nafion nanofiber (400 nm diameter), which is an order of magnitude higher than a bulk Nafion film (ca. 0.1 S cm^{-1}). Also, Wang et al.[14,15] reported on Nafion nanofiber fuel cell electrodes and their subsequent excellent high fuel cell power densities at ultralow platinum loadings (i.e., excellent platinum utilization of 0.076 g kW^{-1}). Additionally, Ballengee and Pintauro[24] fabricated Nafion nanofiber composite membranes by simultaneous dual electrospinning of Nafion and poly(phenyl sulfone) and reported enhanced durability under humidity cycling for fuel cells.

To date, most reports on Nafion nanofibers resulted from the fibers being produced via single needle electrospinning.[14−33,35−41] Needle electrospinning is the most common technique to produce polymer fibers with nanometer sized diameters (ca. 10−1000 nm). This involves applying a high-voltage electric field to a polymer solution that is ejected out of a metal needle. Above a critical voltage, electrostatic forces overcome surface tension to form a polymer jet that is elongated and whipped continuously onto a grounded collector as a randomly interconnected fibrous mat. Electrospinning parameters, such as voltage, distance, and flow rate, can affect how fibers form (i.e., uniformity of the fibers), while polymer solution properties, such as viscosity (i.e., polymer chain entanglement) and conductivity (i.e., electrostatic driving forces), can determine whether a polymer solution can be electrospun to form fibers at all.

Currently, no studies have demonstrated electrospinning of pure Nafion nanofibers, but rather successful electrospinning of Nafion requires the addition of secondary polymer, such as poly(ethylene oxide), poly(acrylic acid), poly(vinylpyrrolidone), poly(vinyl alcohol), and poly(vinylidene fluoride), to the polymer solution prior to electrospinning.[31,35−41] In solution, pure Nafion aggregates into micellar structures, which inhibits polymer chain entanglement and subsequently

Received: July 23, 2019
Accepted: September 3, 2019
Published: September 3, 2019

DOI: 10.1021/acsapm.9b00681
ACS Appl. Polym. Mater. 2019, 1, 2731−2740

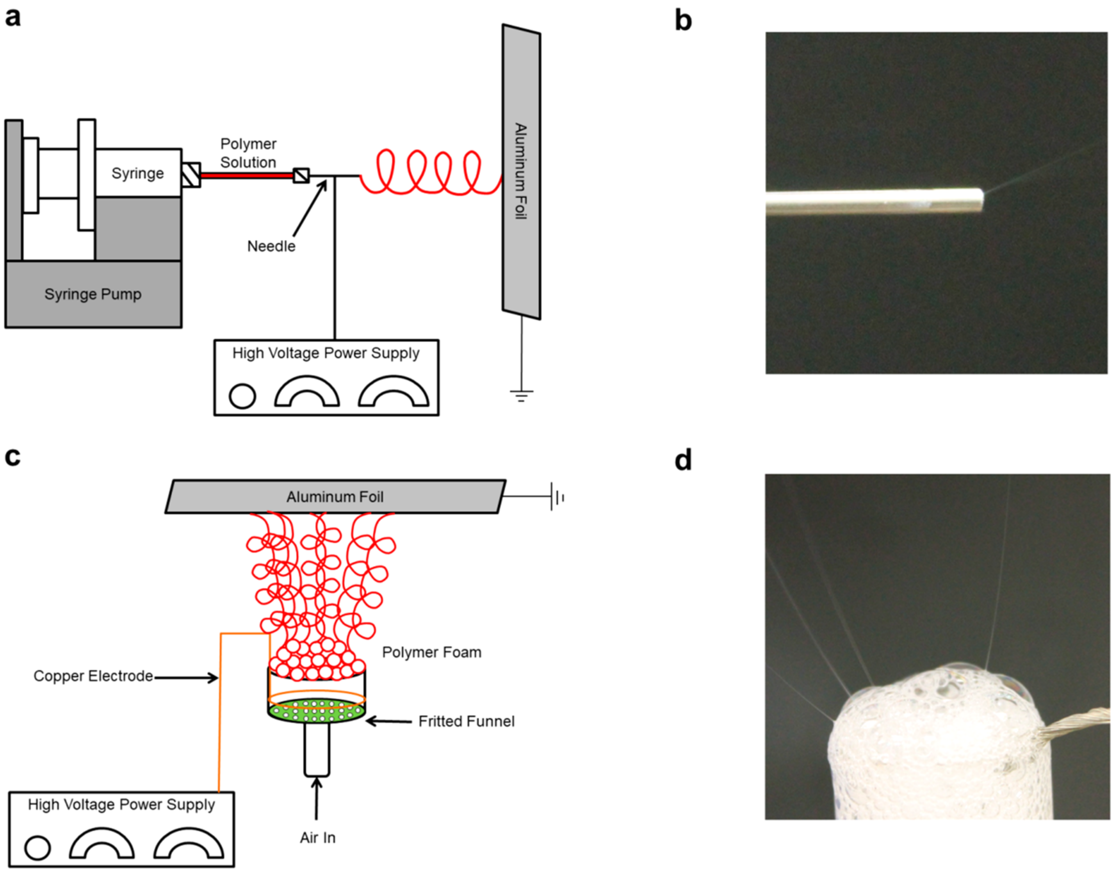

Figure 1. Illustration of (a) needle and (c) needleless electrospinning apparatuses and still images of (b) needle and (d) needleless electrospinning processes.

successful electrospinning.[42] The addition of a secondary polymer (typically 0.1−20 wt % of the solids in the solution) to the Nafion solution has been shown to prevent aggregate formation, increase chain entanglement, and promote the successful electrospinning of Nafion nanofibers.[41] Therefore, it is challenging to electrospin high purity Nafion nanofibers by using conventional needle electrospinning, limiting needle electrospinning to narrow solution concentration ranges and requiring the addition of a secondary polymer.

Furthermore, all of the Nafion electrospinning studies reported to date use single needle electrospinning, which results in low nanofiber production rates (0.01−0.1 g h^{-1}).[43,44] Numerous needleless electrospinning techniques have been developed and explored to increase the production rate of polymer nanofibers, such as upward electrospinning,[45] bubble electrospinning,[46,47] and free surface electrospinning,[43,48] with various polymers, such as poly(vinyl alcohol) and poly(vinylpyrrolidone). These needleless electrospinning techniques have resulted in production rates up to 5 g h^{-1},[48] which is an order of magnitude higher than conventional single needle electrospinning, illustrating the potential to mass produce nanofibers. However, almost all needleless electrospinning techniques produce lower fidelity nanofibers compared to needle electrospinning. Recently, Higham et al.[49] developed a new needleless electrospinning technique, known as foam electrospinning, that produced similar fidelity nanofibers compared to that of needle electrospinning. In their study, they demonstrated this with two neutral polymers: poly(ethylene oxide) and poly(vinyl alcohol). To date, to the authors' knowledge, this study by Higham et al.[49] is the only study to demonstrate foam electrospinning. Higham et al.[49] also demonstrated that the entanglement concentration (i.e., polymer concentration with a sufficient number of chain entanglements to form fibers) is different for poly(vinyl alcohol) and similar for poly(ethylene oxide). However, for poly(ethylene oxide), the formation of smooth fibers occurred at a lower concentration for foam electrospinning (3 wt %) than needle electrospinning (3.5 wt %), which suggests that foam electrospinning can promote the formation of smooth fibers at a slightly lower concentration due to a locally higher polymer concentration at the thin film bubble surface and broaden the narrow concentration ranges specific to electrospinning. In this study, we demonstrate the needleless electrospinning of an ionic polymer, Nafion, using a similar technique described by Higham et al.[49] The production rate, fidelity, purity, and properties of Nafion nanofibers produced by needleless electrospinning were investigated and compared to Nafion nanofibers produced by conventional needle electrospinning.

2. EXPERIMENTAL SECTION

2.1. Materials. Isopropanol (IPA; ACS reagent, ≤99.5%) and poly(acrylic acid) (PAA; M_V = 450000 g mol^{-1}) were purchased from Sigma-Aldrich. The 1100 EW Nafion solutions at 5 wt % in a 3/1 v/v of isopropanol/water and 15 wt % in a 3/1 v/v of isopropanol/water were purchased from Ion Power. All materials were used as received. Deionized (DI) water with a resistivity of 16 MΩ cm was used as appropriate. Dry compressed air was provided using an industrial air compressor (IRN50H-0F, Ingersoll Rand Industrial Technologies).

2.2. Preparation of Nafion Solutions for Electrospinning. Nafion solution (5 wt %) was added to solid PAA and subsequently

DOI: 10.1021/acsapm.9b00681
ACS Appl. Polym. Mater. 2019, 1, 2731−2740

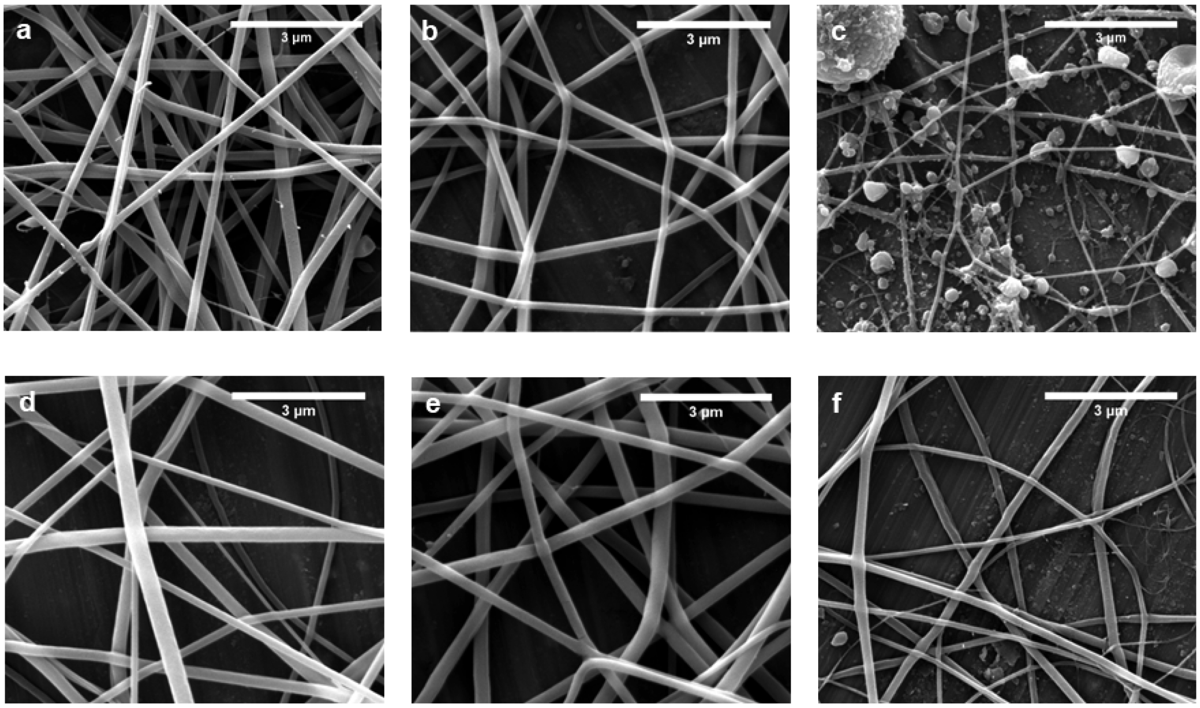

Figure 2. SEM images of electrospun Nafion nanofibers at Nafion contents of 83 wt % (a, d), 88 wt % (b, e), and 92 wt % (c, f) fabricated by using needle electrospinning (a−c) and needleless electrospinning (d−f). Magnification ×30000, scale bar = 3 μm.

stirred under ambient temperature for at least 12 h to ensure complete dissolution. The amount of PAA was adjusted to produce Nafion/PAA solutions of various compositions in order fabricate Nafion content fibers with various Nafion compositions (e.g., 5 g of 5 wt % Nafion solution, 50 mg of PAA for 83 wt % Nafion content of the solids in the electrospinning solution). The 15 wt % Nafion solution was used to produce higher Nafion content (>92 wt %) nanofibers (e.g., 5 g of 15 wt % Nafion solution and 15 mg of PAA for 98 wt % Nafion content of the solids in the electrospinning solution). Isopropanol/water (3/1 v/v) was then added to the Nafion/PAA solution to decrease the polymer concentration (e.g., 1280 mg of Nafion/PAA solution and 670 mg of 3/1 v/v isopropanol/water) for smooth electrospinning.

2.3. Needle Electrospinning Apparatus. The needle electrospinning apparatus, as illustrated in Figure 1a, consists of a high-voltage power supply (PS/EL50R00.8, Glassman High Voltage, Inc.), syringe pump (NE-1000, New Era Pump Systems), glass syringe (Pt. No. CG-3070-03, Chemglass Life Sciences), syringe needle (i.d. = 0.024 in. (0.603 mm), Hamilton), poly(vinyl chloride) tubing (Pt. No. 30600-65, Cole-Parmer), and a grounded collector (9 in. × 9 in. (23 cm × 23 cm); square cardboard covered with aluminum foil). The flow rate was set to 0.3 mL h^{-1} for all needle electrospinning experiments. A still image of the needle electrospinning process (Taylor cone/fiber spinning from syringe needle tip) is shown in Figure 1b.

2.4. Needleless Electrospinning Apparatus. The needleless electrospinning apparatus, as illustrated in Figure 1c, consists of a high-voltage power supply (ES40P-10W/DAM, Gamma High Voltage Research, Inc.), glass fine-fritted funnel (Pt No. CG-1402-04, Chemglass Life Sciences), circular copper electrode (16 gauge wire), and a grounded collector (9 in. × 9 in. (23 cm × 23 cm); square cardboard covered with aluminum foil). Compressed air with controlled flow rate was passed through the funnel to produce stable polymeric foam at the top surface of the fritted funnel. A still image of the needless electrospinning process (multiple Taylor cones/fiber spinning from polymeric foam/bubble surfaces) is shown in Figure 1d.

2.5. Characterization. The morphology of the fiber mats was investigated with scanning electron microscopy (SEM; FEI Quanta 600 FE-SEM, 10 kV for 30000× magnification images) using a working distance of 10 mm. Samples were sputter coated (Cressington 208 HR) with platinum/palladium (6 nm thickness) prior to SEM analysis. For each electrospinning experiment, the diameters of 25 nanofibers for each image were randomly selected and measured by using ImageJ software; i.e., fiber diameters reported are the average and standard deviation of 25 randomly selected fibers.

The production rate was determined by the amount of material collected after the electrospinning experiments at different time points. Foil circles were punched out by using a hollow punch (diameter = 14 mm, Pt. 66004, Mayhew Pro). The average weight of six bare aluminum foil circles (6.6 mg) was used to tare the weight at t = 0 h. The average weight of four to six samples at different time intervals was taken from each electrospinning experiment to determine the weight after the experiment as a function of time. The total collection time was approximately 0.3−2.5 h for the needleless electrospinning and 6−8 h for the needle electrospinning. The production rate was measured as the weight of the sample/electrospinning time/area required to electrospin (mg h^{-1} m^{-2}). The required electrospinning area (i.e., area required to electrospin) for the needle apparatus includes the surrounding area between needles (nozzles) to avoid electrospinning interferences due to nearby electrical fields from each needle. Commercial multineedle electrospinning systems typically report distances of ∼5 cm between needles. The required electrospinning area for the needleless electrospinning was calculated by using the surface area of the funnel (for this study i.d. = ca. 11.44 mm). Therefore, the required electrospinning areas for needle electrospinning and needleless electrospinning were calculated via $A = \pi r^2$, where r is the distance between nozzles and the radius of the funnel, respectively.

Mechanical properties of the fiber mats (ca. 25 mm (L) × 0.5 mm (W)) were measured with dynamic mechanical analysis (DMA; Q800, TA Instruments) under the given conditions: 22 ± 2 °C, 40 ± 5% RH, preload force of 0.001 N, and a strain ramp rate of 0.1% min^{-1}. Stress−strain profiles were collected for each sample. The Young's modulus was measured from the initial slope of the stress−strain curve.

In-plane ionic conductivity of the fiber mats was measured with electrochemical impedance spectroscopy (EIS; Solartron SI 1260A)

DOI: 10.1021/acsapm.9b00681
ACS Appl. Polym. Mater. 2019, 1, 2731−2740

in a four-point conductivity cell (BekkTech BT112, Scribner Associates, Inc.) by sweeping frequencies from 1 MHz to 0.05 Hz with an amplitude of 10 mV at 0 V versus OCV under different temperatures ranging from 30 to 80 °C at 90% RH and submersed in liquid DI water at room temperatures (ca. 25 ± 2 °C). The temperature and relative humidity were controlled by placing the four-point conductivity cell in a benchtop environmental chamber (ESPEC). Samples for EIS were prepared by electrospinning on glass substrates (ca. 30 mm (L) × 8 mm (W) × 1 mm (T)) for fiber mats. A film was cast on glass substrates and dried for at least 24 h under ambient conditions to compare to the fiber mats. All samples were annealed at 140 °C for 15 min prior to testing the in-plane conductivities. The data were analyzed by determining the high-frequency intercept of the real impedance, R, which was measured between the two inner reference electrodes. The conductivity was calculated by using the following equation: $\sigma = L/(AR)$, where L is the distance between the two inner electrodes (ca. 0.48 mm) and A is the cross-sectional area of the sample ($A = Wl$; W is the sample width and l is the sample thickness). The sample thicknesses, ranging from 20 to 60 μm, were measured with a Marathon digital micrometer (Pt No. CO030025) with ±2 μm accuracy. Samples were allowed to equilibrate for 2 h at each temperature at 90% RH followed by three to four repeated measurements. The reported values are the average of these measurements. Because of the porosity of the fiber mats, the effective conductivity was calculated via the following equation: $\sigma_c = \sigma A/A_c = \sigma/(1 - \nu)$, where σ is the measured conductivity, A_c is the effective surface area (surface area covered by the fibers), and ν is the surface area void fraction, or surface porosity, of the fiber mats. The surface porosity was measured by using similar techniques described by Liu et al.[50] and Hotaling et al.[51] Assuming the fiber mats are isotropic, the in-plane surface void area fraction of the fiber mat was used to determine the cross-sectional void area fraction. The average of the in-plane surface void area fractions for two different SEM images was used for the final calculation for each fiber mat.

3. RESULTS AND DISCUSSION

Figure 2 shows scanning electron microscopy images of Nafion nanofibers produced from both the needle electrospinning technique (Figure 2a−c) and the needleless electrospinning technique (Figure 2d−f) at various Nafion contents of the solids in the electrospinning solution (83, 88, and 92 wt %). At 83 and 88 wt % Nafion content, both needle and needleless electrospinning techniques can produce uniform defect-free fibers. However, by use of the needle electrospinning technique, as the amount of Nafion content of the solids in the Nafion/PAA solution increases from 88 wt % (Figure 2b) to 92 wt % (Figure 2c), the fibers begin to show defects, such as beads, whereas the needleless electrospinning technique still produces defect-free fibers (Figure 2f). This beaded fiber-to-smooth fiber transition has been previously reported by Chen et al.[41] with the needle electrospinning technique at 92 wt % Nafion content of the solids in the solution. Therefore, although both electrospinning techniques are using the same polymer solution, at a higher Nafion content solution, the needle electrospinning technique produces a lower quality of nanofibers (e.g., beaded nanofibers), whereas the needleless electrospinning technique fabricates defect-free nanofibers at the same higher Nafion concentrations. These results suggest that the needleless electrospinning technique enhances electrospinning, which may be a result of increasing the polymer concentration locally on the polymer solution thin bubble surfaces (foam).

Previous studies have shown that higher polymer concentrations (concentrations above the polymer entanglement concentration) promote the formation of uniform, bead-free fibers produced via electrospinning.[49,52] Therefore, to promote the electrospinning of higher purity Nafion solutions, the polymer concentrations were increased to 10 and 6 wt % to electrospin 95 and 98 wt % Nafion content of the solids in the solution, respectively. As shown in Figure 3a,c, both techniques can produce nanofibers for the 95 wt % Nafion content of the solids in the solution at 10 wt % polymer concentration. However, needle electrospinning produces beaded nanofibers at this polymer concentration, as shown in Figure 3a, whereas needleless electrospinning produces bead-free or defect-free nanofibers, as shown in Figure 3c. Also, the needle electrospinning technique requires frequent monitoring and clearing at the needle tip to inhibit solution clogging and noncontinuous electrospinning of fibers for this polymer solution. At 98 wt % Nafion content of the solids in a 6 wt % polymer solution, needle electrospinning produces multiple beads with few small fibers in between the beads, as shown in Figure 3b, whereas needleless electrospinning can still produce bead-free fibers, as shown in Figure 3d. These results demonstrate that needleless electrospinning produces higher purity defect-free Nafion nanofibers compared to needle electrospinning due to the increase in local polymer concentration at the bubble surfaces.

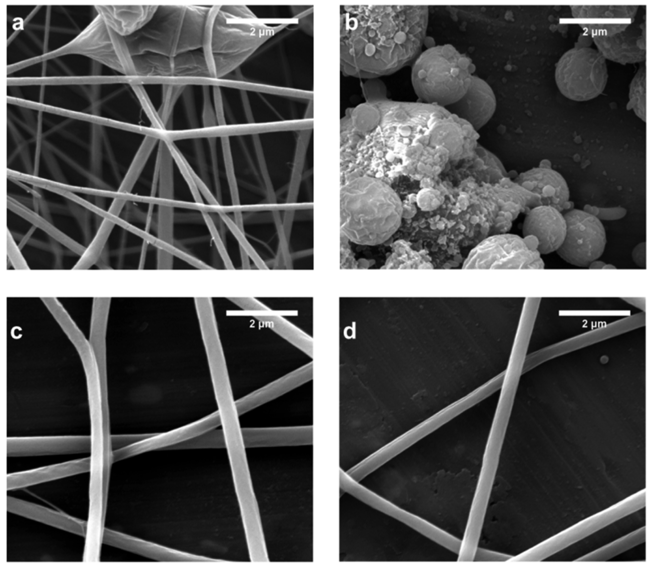

Figure 3. SEM images of Nafion nanofibers at Nafion contents of 95 wt % (a, c) and 98 wt % (b, d) fabricated using needle electrospinning (a, b) and needleless electrospinning (c, d). Magnification ×30000 , scale bar = 2 μm.

Figure 4a shows the average fiber diameters of the images shown in Figure 2. The average fiber diameters for the 83, 88, and 92 wt % Nafion content of the solids in the solution fabricated by using the needle electrospinning technique are 216, 130, and 110 nm, respectively. The average fiber diameters for 83, 88, and 92 wt % Nafion content of the solids in the solution fabricated by using the needleless electrospinning technique are 233, 179, and 156 nm, respectively. Figures 4b, 4c, and 4d show the histograms of the fiber diameters for the 83, 88, and 92 wt % Nafion content of the solids in the solution, respectively. Overall, distributions between needle and needleless techniques are fairly similar to slightly more higher fiber counts from the needleless compared to the needle as Nafion content increases (88 and 92 wt %). The needle and needleless electrospinning techniques both

DOI: 10.1021/acsapm.9b00681
ACS Appl. Polym. Mater. 2019, 1, 2731−2740

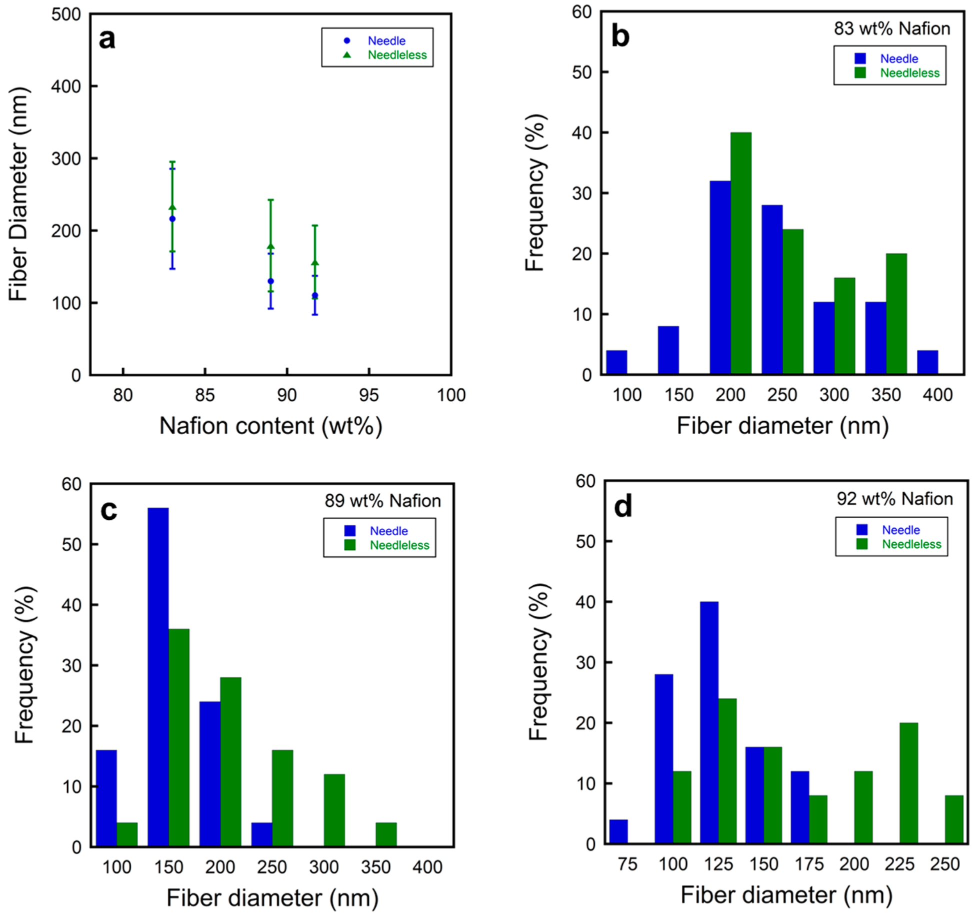

Figure 4. (a) Nafion nanofiber diameters as a function of Nafion content and (b−d) histograms of nanofiber diameters fabricated by using needle electrospinning (blue circles) and needleless electrospinning (green triangles). Nafion contents: (b) 83, (c) 89, and (d) 92 wt %.

produced similar diameter size fibers (i.e., similar fidelity) for various Nafion contents of the solids in the solution. Both techniques also display similar trends in decreasing fiber diameter with increasing Nafion content, which is in agreement with the electrospinning of Nafion and PAA study by Chen et al.,[41] where nanofiber diameters ranging from 90 to 600 nm for a PAA content of 8 to 100 wt %, respectively, were reported.[41,52] Thus, needleless electrospinning can produce similar fidelity (i.e., similar fiber diameter size and size distribution) Nafion nanofibers as those produced by needle electrospinning at 83 wt % Nafion content and higher quality (i.e., less beaded fibers) at >83 wt % Nafion content than those produced by needle electrospinning.

Figure 5 shows the effect of various electrospinning parameters on the resulting fiber diameters for the needleless electrospinning technique, including polymer concentration (wt %), funnel-to-target distance (cm), and voltage (kV). Results show that the average fiber diameter for 4.0, 5.0, and 5.9 wt % polymer solutions is 216, 252, and 232 nm, respectively (see Figure 5a). These average fiber diameters are similar, which demonstrates the ability of the needleless electrospinning technique to produce similar fiber diameters with different polymer concentrations. In Figure 5b, the funnel-to-target distance was varied from 13, 15, and 17 cm, and the resulting fiber diameters are 392, 232, and 326 nm. Using a distance of 13 or 17 cm resulted in a higher standard deviation in the fiber diameter compared to that using a distance of 15 cm, suggesting that at 20 kV, 15 cm is the optimal distance for maintaining high fidelity fibers with similar diameter sizes. The applied voltage was varied from 15, 20, and 25 kV, and the resulting fiber diameters are 375, 232, and 292 nm (see Figure 5c). Applying a voltage of 20 or 25 kV resulted in higher standard deviation in the fiber diameter compared to that using a voltage of 15 kV, suggesting that at 15 cm, 15 kV is the optimal voltage for fabricating similar fiber diameter sizes. By changing electrospinning parameters, such as distance and voltage, the fiber diameters can vary, but by fixing one parameter and optimizing the other parameters, there is a combination that offers the highest fidelity in nanofibers produced by using the needleless electrospinning technique.

Figure 6 shows the production rate of nanofibers fabricated by using both the needle and needleless electrospinning techniques. The production rate for needle electrospinning ranges from 11 to 20 mg h^{-1} m^{-2} across a voltage range from 10 to 30 kV. From 10 to 20 kV, the needle electrospinning production rate is constant around 11−14 mg h^{-1} m^{-2} followed by a slight increase to 20 mg h^{-1} m^{-2} at 30 kV. The production rate for the needleless electrospinning technique ranges from 422 to 9729 mg h^{-1} m^{-2} across a voltage range from 10 to 30 kV. At 15 kV, the production rate for the needleless electrospinning technique is 3316 mg h^{-1} m^{-2}. From 15 to 20 kV, the production rate for needleless electrospinning increases to 5437 mg h^{-1} m^{-2}. From 20 to 25 kV, the production rate for the needleless electrospinning technique further increases to 9729 mg h^{-1} m^{-2}. At 30 kV, the production for the needleless electrospinning technique

DOI: 10.1021/acsapm.9b00681
ACS Appl. Polym. Mater. 2019, 1, 2731−2740

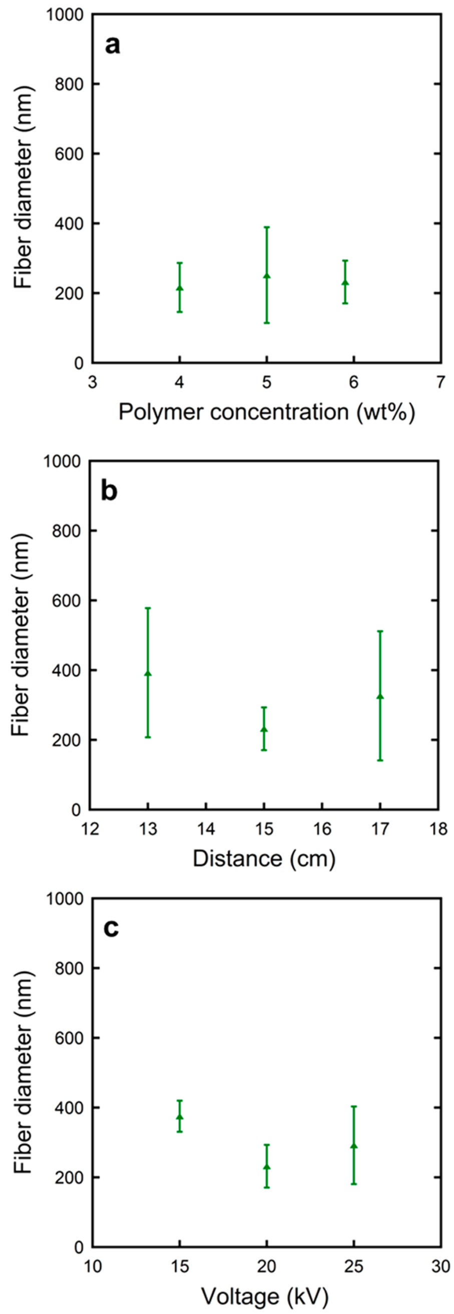

Figure 5. Nafion nanofiber diameters fabricated using needleless electrospinning as a function of (a) polymer concentration, (b) funnel-to-target distance, and (c) voltage.

decreases to 6633 mg h^{-1} m^{-2}. This decrease may be due to the strong electric field pulling the fibers from the surface faster than the production of the polymeric foam or curved surfaces. Comparing the two electrospinning techniques, at 10 kV, the production rate for needle electrospinning (14 mg h^{-1} m^{-2}) is an order of magnitude lower than that for needleless electrospinning (422 mg h^{-1} m^{-2}). At 20 kV, the production rate of needleless electrospinning (5437 mg h^{-1} m^{-2}) is almost an order of magnitude higher than at 10 kV, which suggests that although there are multiple available curved surfaces for electrospinning, the voltage is not high enough to efficiently produce many Taylor cone jets for all the curved surfaces. At 25 kV, the needleless electrospinning production rate reaches its maximum at 9729 mg h^{-1} m^{-2}, 2 orders of magnitude

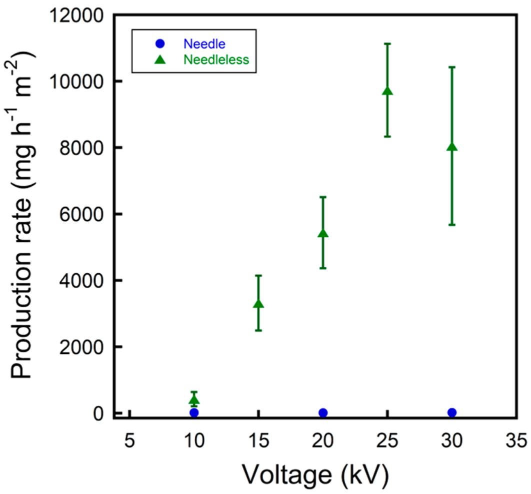

Figure 6. Nafion nanofiber production rate as a function of voltage for needle electrospinning (blue circles) and needleless electrospinning (green triangles).

higher than the needle electrospinning production rates, demonstrating the ability of using the needleless electrospinning technique to quickly fabricate many nanofibers. Therefore, there is an optimum voltage for the maximum production rate for needleless electrospinning, whereas the production rate for needle electrospinning remains relatively constant with increasing voltage. Overall, needleless electrospinning can produce Nafion nanofibers at 2 orders of magnitude higher production rate compared to needle electrospinning.

In addition to purity, fidelity, and production rate, the physical properties of the resulting fiber mats produced by both needle and needleless electrospinning techniques were compared with one another and also compared to the bulk film (a control with similar Nafion/PAA composition as fibers). Table 1 lists the Young's modulus and proton conductivity for the film and the fiber mats for a composition of 83 wt % Nafion.

Table 1. Properties for Fiber Mats and Cast Film at 83 wt % Nafion Content

fabrication	Young's modulus[a] (MPa)	conductivity[b] (mS cm^{-1})
cast film	130.0	54.3 ± 0.3
needle fiber mat	20.9	18.0 ± 0.1
needleless fiber mat	42.6	43.8 ± 0.9

[a]Measured under ambient conditions (ca. 22 ± 2 °C, 40 ± 5% RH). [b]Measured submersed in liquid deionized water at room temperature (ca. 25 ± 2 °C).

Overall, as expected, the film has a higher modulus (130.0 MPa) and proton conductivity (54.3 mS cm^{-1}) compared to both fiber mats. However, unexpectedly, the needleless electrospun fiber mat has a higher modulus (42.6 MPa) and proton conductivity (43.8 mS cm^{-1}) compared to the needle electrospun fiber mat (20.9 MPa and 18.0 mS cm^{-1}). One would expect that although the fibers were produced by different techniques that if their fidelities are similar, then the properties should also be similar. However, at this composition, beaded fibers were observed for the needle electrospun fibers (shown in Figure 7a) compared to defect-free fibers in the needleless electrospun fibers (shown in Figure

DOI: 10.1021/acsapm.9b00681
ACS Appl. Polym. Mater. 2019, 1, 2731−2740

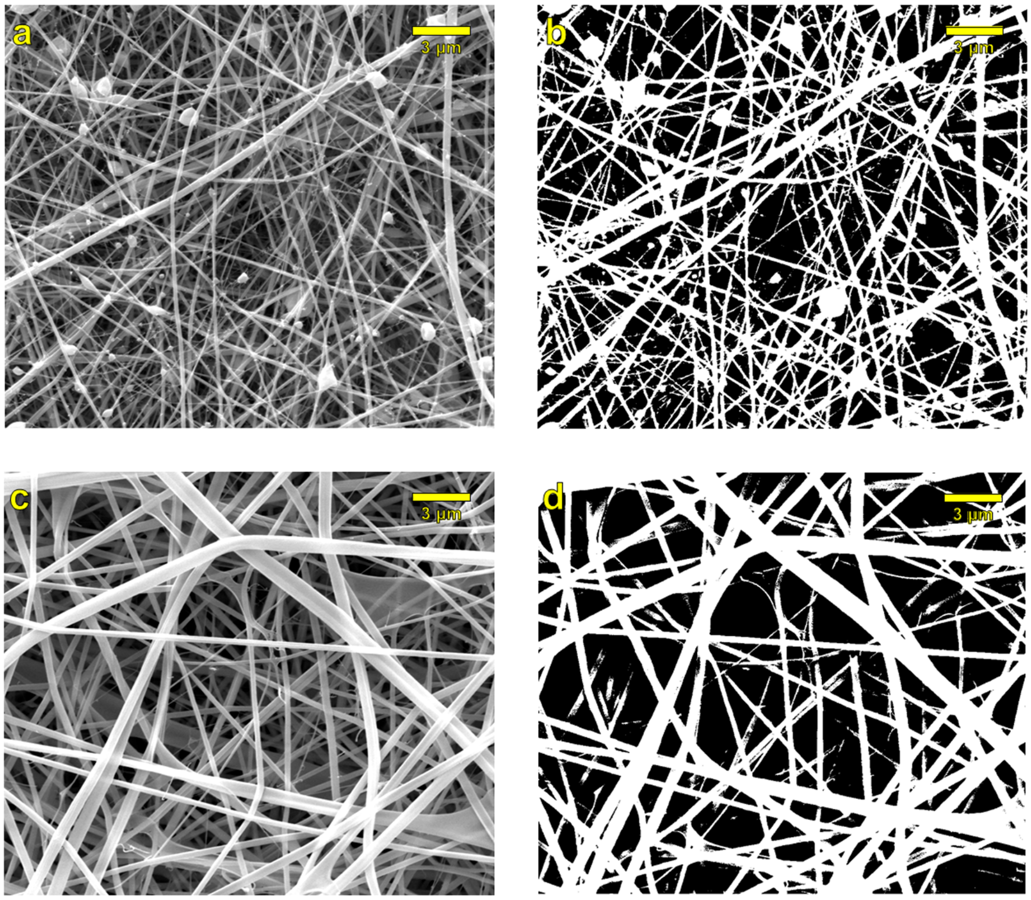

Figure 7. SEM images (a, c) and contrast images (b, d) of Nafion nanofibers at 83 wt % Nafion content of the solids in the electrospinning solution fabricated using (a, b) needle electrospinning and (c, d) needleless electrospinning. Magnification ×10000 , scale bar = 3 μm.

7c). The defects in the needle electrospun fibers may contribute to the differences in measured properties when compared to the defect-free needleless electrospun fibers.

More specifically, Figure 8 shows the stress−strain profiles (mechanical properties) for the needle and needleless electrospun fiber mats and the control film. Tensile strength trends are similar to the Young's modulus, where the needle electrospun fiber mat (0.8 MPa) is lower than the needleless electrospun fiber mat (2.4 MPa) and the film (5.7 MPa) is higher than both electrospun mats. It is expected that the mechanical properties of a dense film would be higher than a porous fiber mat. The elongation-to-break is similar for all samples (6.5% for needle electrospun fiber mat, 10.7% for needleless electropsun fiber mat, and 6.5% for dense film). Thus, needleless electrospinning can produce higher purity defect-free Nafion nanofibers, which results in improved mechanical properties and liquid-saturated proton conductivity when compared to beaded fibers from needle electrospinning at a similar composition.

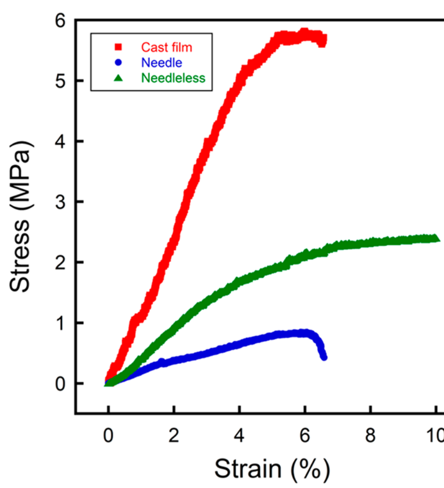

Figure 8. Stress−strain profiles for cast film (red squares), needle electrospun nanofiber mat (blue circles), and needleless electrospun nanofiber mat (green triangles).

Figure 9a shows the proton conductivity for the needle and needleless electrospun fiber mats and the control film at 90% relative humidity as a function of temperature (ranging from 30 to 80 °C). Similar to the results listed in Table 1 (submersed in liquid water at room temperature), the proton conductivity at 80 °C and 90% RH for the film (69.9 mS cm^{-1}) is higher than the needleless fiber mat (51.8 mS cm^{-1}), which is higher than the needle electrospun fiber mat (24.4 mS cm^{-1}). The conductivities measured in this study for needle electrospun Nafion fiber mats are similar to those reported in other studies.[19,22,24−26,53,54] However, the cross-sectional area used to calculate conductivity from the impedance data assumes that the entire area is conducting medium, which is only the case for the solid dense film and not the porous fiber mats. In an attempt to normalize the data (i.e., only the area of the conducting solid polymer), an estimated surface area porosity was measured from the SEM images. The contrast

DOI: 10.1021/acsapm.9b00681
ACS Appl. Polym. Mater. 2019, 1, 2731−2740

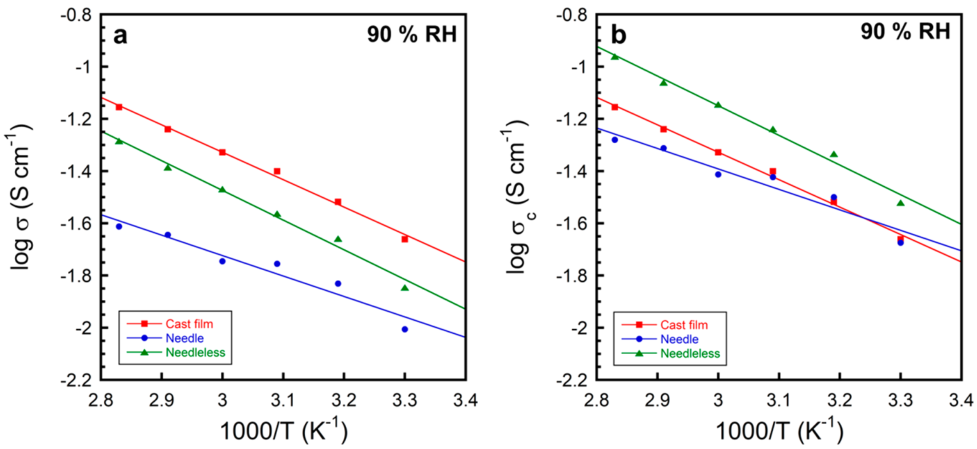

Figure 9. (a) Proton conductivity and (b) normalized proton conductivity as a function of temperature at 90% relative humidity for cast film (red squares), needle electrospun nanofiber mat (blue circles), and needleless electrospun nanofiber mat (green triangles). Solid lines represent a regression to the Arrhenius model.

feature in ImageJ was used to distinguish between solid and pores in the mat (see Figures 7b and 7d, which are contrasts of Figures 7a and 7c, respectively). From this method, the average void area fractions of the needle and needleless electrospun fiber mats were similar at 53.4% and 52.7%, respectively. These estimated surface area porosities were used to calculate a corrected surface area for the fiber mats (area of only the conducting solid) and subsequently a normalized conductivity. Figure 9b shows the normalized proton conductivity of the data shown in Figure 9a for the needle and needleless electrospun fiber mats and the control film. Here, the proton conductivity at 80 °C and 90% RH for needleless fiber mat (109 mS cm^{-1}) is higher than the dense film (70 mS cm^{-1}), which is higher than the needle electrospun fiber mat (52 mS cm^{-1}).

This data are supported by a previous study by Dong et al.,[31] which reported on the proton conductivity of a single high-purity Nafion nanofiber at a value that was an order of magnitude higher than a cast Nafion dense film. They attributed this to the high alignment of connected nanoscale ionic network along the fiber axis (supported by small-angle X-ray scattering). Dong et al.[31] reported a conductivity of 1.5 S cm^{-1} for a single 99.9 wt % Nafion nanofiber (400 nm in diameter) at 30 °C and 90% RH. In comparison, in this study, the normalized conductivity for multiple 83.0 wt % Nafion nanofibers (average 233 nm in diameter) is 30 mS cm^{-1}. The differences in proton conductivity between these two studies could be the result of differences in Nafion content as well as differences in measuring a single fiber versus many fibers (where an effective surface area correction is used in the latter). The solid lines in Figure 9 represent a regression to the Arrhenius equation, where the activation energies were determined to be similar for all samples (8.7, 9.4, and 6.5 kJ mol^{-1} for film, needleless, and needle fiber mat, respectively). These results are similar to other reports of Nafion proton conductivity activation energies.[54] Thus, needleless electrospinning can produce high purity Nafion nanofibers with improved proton conductive properties compared with needle electrospun Nafion nanofibers and solution cast Nafion films.

4. CONCLUSIONS

In this study, the needleless electrospinning of the highly ionic polymer Nafion was demonstrated, and the results were compared to a classic needle-based electrospinning process. Needleless electrospinning produced Nafion nanofibers (233 ± 62 nm) with similar fidelity to those produced by needle electrospinning (216 ± 69 nm). Needleless electrospinning produced higher purity Nafion nanofibers (98 wt % Nafion) compared to needle electrospinning, where no fibers (only beads) were produced at this similar polymer solution concentration. Needleless electrospinning produced Nafion nanofibers at 2 orders of magnitude higher production rate compared to needle electrospinning (9729 vs 14 mg h^{-1} m^{-2}). Both high productivity and high purity were afforded through the ability of this needleless electrospinning process to generate multiple electrospinning sites that promote chain entanglement for facile electrospinning due to the locally higher polymer concentrations at thin bubble surface solution sites. The needleless electrospinning allows for locally higher polymer concentration solution in an open system without impeding the formation of nanofibers with a narrow needle electrospinning. Also, the Nafion nanofiber mats produced by needleless electrospinning resulted in enhanced Young's modulus and proton conductivity (42.6 MPa and 43.8 mS cm^{-1}, respectively) compared to those produced with needle electrospinning (20.9 MPa and 18.0 mS cm^{-1}). Overall, this work not only demonstrates the ability to produce high fidelity, high purity Nafion nanofibers at high production rates and improved properties using needleless electrospinning but also extends the capability of foam electrospinning to highly ionic polymers, while maintaining high fidelity and higher production rates. Furthermore, the results from this work motivate future studies on the needleless electrospinning of other ion-containing polymers and future fundamental studies on the polymer physics of polyelectrolyte solutions at thin film surfaces under applied electric fields.

■ ASSOCIATED CONTENT

Supporting Information

The Supporting Information is available free of charge on the ACS Publications website at DOI: 10.1021/acsapm.9b00681.

Video of needleless electrospinning of Nafion (MPG)

■ AUTHOR INFORMATION

Corresponding Author

*E-mail: elabd@tamu.edu.

DOI: 10.1021/acsapm.9b00681
ACS Appl. Polym. Mater. 2019, 1, 2731–2740

ORCID

Yossef A. Elabd: 0000-0002-7790-9445

Notes

The authors declare no competing financial interest.

■ ACKNOWLEDGMENTS

This work was supported in part by the National Science Foundation under Award CMMI-1661822. The FE-SEM acquisition was supported by the NSF Grant DBI-0116835, the VP for Research Office, and the TX Eng. Exp. Station.

■ REFERENCES

(1) Grot, W. Use of Nafion Perfluorosulfonic Acid Products as Separators in Electrolytic Cells. *Chem. Ing. Technol.* **1978**, *50*, 299−301.

(2) Chandran, R. R.; Chin, D. T. Reactor Analysis of a Chlor Alkali Membrane Cell. *Electrochim. Acta* **1986**, *31*, 39−50.

(3) Coo, L. D.; Martinez, I. S. Nafion-Based Optical Sensor for the Determination of Selenium in Water Samples. *Talanta* **2004**, *64*, 1317−1322.

(4) Wu, R. J.; Sun, Y. L.; Lin, C. C.; Chen, H. W.; Chavali, M. Composite of TiO_2 Nanowires and Nafion as Humidity Sensor Material. *Sens. Actuators, B* **2006**, *115*, 198−204.

(5) Madden, J. E.; Cardwell, T. J.; Cattrall, R.; Deady, L. W. Nafion-Based Optode for the Detection of Metal Ions in Flow Analysis. *Anal. Chim. Acta* **1996**, *319*, 129−134.

(6) Gelbard, G. Organic Synthesis by Catalysis with Ion-Exchange Resins. *Ind. Eng. Chem. Res.* **2005**, *44*, 8468−8498.

(7) Konishi, H.; Suetsugu, K.; Okano, T.; Kiji, J. The Nafion-H-Catalyzed Acylation of Thiophene with Acid Anhydrides. *Bull. Chem. Soc. Jpn.* **1982**, *55*, 957−958.

(8) Yamato, T.; Hideshima, C.; Prakash, G. K. S.; Olah, G. A. Organic-Reactions Catalyzed by Solid Superacids 0.5. Perfluorinated Sulfonic-Acid Resin (Nafion-H) Catalyzed Intramolecular Friedel-Crafts Acylation. *J. Org. Chem.* **1991**, *56*, 3955−3957.

(9) Banerjee, S.; Curtin, D. E. Nafion (R) Perfluorinated Membranes in Fuel Cells. *J. Fluorine Chem.* **2004**, *125*, 1211−1216.

(10) Srinivasan, S.; Ticianelli, E. A.; Derouin, C. R.; Redondo, A. Advances in Solid Polymer Electrolyte Fuel-Cell Technology with Low Platinum Loading Electrodes. *J. Power Sources* **1988**, *22*, 359−375.

(11) Wilson, M. S.; Gottesfeld, S. Thin-Film Catalyst Layers for Polymer Electrolyte Fuel-Cell Electrodes. *J. Appl. Electrochem.* **1992**, *22*, 1−7.

(12) Passalacqua, E.; Lufrano, F.; Squadrito, G.; Patti, A.; Giorgi, L. Nafion Content in the Catalyst Layer of Polymer Electrolyte Fuel Cells: Effects on Structure and Performance. *Electrochim. Acta* **2001**, *46*, 799−805.

(13) Sasikumar, G.; Ihm, J. W.; Ryu, H. Optimum Nafion Content in Pem Fuel Cell Electrodes. *Electrochim. Acta* **2004**, *50*, 601−605.

(14) Wang, X.; Richey, F. W.; Wujcik, K. H.; Elabd, Y. A. Ultra-Low Platinum Loadings in Polymer Electrolyte Membrane Fuel Cell Electrodes Fabricated Via Simultaneous Electrospinning/Electrospraying Method. *J. Power Sources* **2014**, *264*, 42−48.

(15) Wang, X.; Richey, F. W.; Wujcik, K. H.; Ventura, R.; Mattson, K.; Elabd, Y. A. Effect of Polytetrafluoroethylene on Ultra-Low Platinum Loaded Electrospun/Electrosprayed Electrodes in Proton Exchange Membrane Fuel Cells. *Electrochim. Acta* **2014**, *139*, 217−224.

(16) Brodt, M.; Wycisk, R.; Dale, N.; Pintauro, P. Power Output and Durability of Electrospun Fuel Cell Fiber Cathodes with Pvdf and Nafion/Pvdf Binders. *J. Electrochem. Soc.* **2016**, *163*, F401−F410.

(17) Brodt, M.; Wycisk, R.; Pintauro, P. N. Nanofiber Electrodes with Low Platinum Loading for High Power Hydrogen/Air Pem Fuel Cells. *J. Electrochem. Soc.* **2013**, *160*, F744−F749.

(18) Ballengee, J. B.; Pintauro, P. N. Preparation of Nanofiber Composite Proton-Exchange Membranes from Dual Fiber Electrospun Mats. *J. Membr. Sci.* **2013**, *442*, 187−195.

(19) Lee, K. M.; Choi, J.; Wycisk, R.; Pintauro, P. N.; Mather, P. T. Nafion Nanofiber Membranes. *Proton Exchange Membrane Fuel Cells 9* **2009**, *25*, 1451−1458.

(20) Hasani-Sadrabadi, M. M.; Shabani, I.; Soleimani, M.; Moaddel, H. Novel Nanofiber-Based Triple-Layer Proton Exchange Membranes for Fuel Cell Applications. *J. Power Sources* **2011**, *196*, 4599−4603.

(21) Shabani, I.; Hasani-Sadrabadi, M. M.; Haddadi-Asl, V.; Soleimani, M. Nanofiber-Based Polyelectrolytes as Novel Membranes for Fuel Cell Applications. *J. Membr. Sci.* **2011**, *368*, 233−240.

(22) Laforgue, A.; Robitaille, L.; Mokrini, A.; Ajji, A. Fabrication and Characterization of Ionic Conducting Nanofibers. *Macromol. Mater. Eng.* **2007**, *292*, 1229−1236.

(23) Brodt, M.; Han, T.; Dale, N.; Niangar, E.; Wycisk, R.; Pintauro, P. Fabrication, in-Situ Performance, and Durability of Nanofiber Fuel Cell Electrodes. *J. Electrochem. Soc.* **2015**, *162*, F84−F91.

(24) Ballengee, J. B.; Pintauro, P. N. Composite Fuel Cell Membranes from Dual-Nanofiber Electrospun Mats. *Macromolecules* **2011**, *44*, 7307−7314.

(25) Simotwo, S.; Kalra, V. Dual Nafion/Polyaniline Nanofibers Architecture for Applications in Fuel Cells Electrodes. *ECS Trans.* **2015**, *69*, 943−953.

(26) Park, J. W.; Wycisk, R.; Pintauro, P. N.; Yarlagadda, V.; Nguyen, T. V. Electrospun Nafion (R)/Polyphenylsulfone Composite Membranes for Regenerative Hydrogen Bromine Fuel Cells. *Materials* **2016**, *9*, 143−143.

(27) Tran, C.; Kalra, V. Fabrication of Porous Carbon Nanofibers with Adjustable Pore Sizes as Electrodes for Supercapacitors. *J. Power Sources* **2013**, *235*, 289−296.

(28) Sheng, L.; Dajing, C.; Yuquan, C. A Surface Acoustic Wave Humidity Sensor with High Sensitivity Based on Electrospun Mwcnt/Nafion Nanofiber Films. *Nanotechnology* **2011**, *22*, 265504−265504.

(29) Okafor, C.; Maaza, M.; Mokrani, T. Nafion Nanofiber Composite Membrane Fabrication for Fuel Cell Applications. *Int. J. Chem. Nucl. Mater. Metall Eng.* **2014**, *8*, 389−392.

(30) Lee, J.-W.; Yoo, Y.-T. Preparation and Performance of Ipmc Actuators with Electrospun Nafion®−Mwnt Composite Electrodes. *Sens. Actuators, B* **2011**, *159*, 103−111.

(31) Dong, B.; Gwee, L.; Salas-de la Cruz, D.; Winey, K. I.; Elabd, Y. A. Super Proton Conductive High-Purity Nafion Nanofibers. *Nano Lett.* **2010**, *10*, 3785−3790.

(32) Zhang, F.; Zhang, Z.; Liu, Y.; Leng, J. Shape Memory Properties of Electrospun Nafion Nanofibers. *Fibers Polym.* **2014**, *15*, 534−539.

(33) Zhang, F.; Zhang, Z.; Liu, Y.; Lu, H.; Leng, J. The Quintuple-Shape Memory Effect in Electrospun Nanofiber Membranes. *Smart Mater. Struct.* **2013**, *22*, 085020−085020.

(34) Snyder, J. D.; Elabd, Y. A. Nafion (R) Nanofibers and Their Effect on Polymer Electrolyte Membrane Fuel Cell Performance. *J. Power Sources* **2009**, *186*, 385−392.

(35) Bajon, R.; Balaji, S.; Guo, S. M. Electrospun Nafion Nanofiber for Proton Exchange Membrane Fuel Cell Application. *J. Fuel Cell Sci. Technol.* **2009**, *6*, 031004−031004.

(36) Zhang, W. J.; Pintauro, P. N. High-Performance Nanofiber Fuel Cell Electrodes. *ChemSusChem* **2011**, *4*, 1753−1757.

(37) Pan, C.; Wu, H.; Wang, C.; Wang, B.; Zhang, L.; Cheng, Z.; Hu, P.; Pan, W.; Zhou, Z.; Yang, X.; Zhu, J. Nanowire-Based High-Performance "Micro Fuel Cells": One Nanowire, One Fuel Cell. *Adv. Mater.* **2008**, *20*, 1644−1648.

(38) Park, J. W.; Wycisk, R.; Lin, G. Y.; Chong, P. Y.; Powers, D.; Van Nguyen, T.; Dowd, R. P.; Pintauro, P. N. Electrospun Nafion/Pvdf Single-Fiber Blended Membranes for Regenerative H-2/Br-2 Fuel Cells. *J. Membr. Sci.* **2017**, *541*, 85−92.

(39) Ballengee, J. B.; Pintauro, P. N. Morphological Control of Electrospun Nafion Nanofiber Mats. *J. Electrochem. Soc.* **2011**, *158*, B568−B572.

DOI: 10.1021/acsapm.9b00681
ACS Appl. Polym. Mater. 2019, 1, 2731−2740

(40) Song, T. D.; Chen, Z. Y.; He, H.; Liu, Y. X.; Liu, Y.; Ramakrishna, S. Orthogonal Design Study on Factors Affecting the Diameter of Perfluorinated Sulfonic Acid Nanofibers During Electrospinning. *J. Appl. Polym. Sci.* **2015**, *132*, 41755−41755.
(41) Chen, H.; Snyder, J. D.; Elabd, Y. A. Electrospinning and Solution Properties of Nafion and Poly(Acrylic Acid). *Macromolecules* **2008**, *41*, 128−135.
(42) Welch, C.; Labouriau, A.; Hjelm, R.; Orler, B.; Johnston, C.; Kim, Y. S. Nafion in Dilute Solvent Systems: Dispersion or Solution? *ACS Macro Lett.* **2012**, *1*, 1403−1407.
(43) Varabhas, J. S.; Chase, G. G.; Reneker, D. H. Electrospun Nanofibers from a Porous Hollow Tube. *Polymer* **2008**, *49*, 4226−4229.
(44) Salem, D. Electrospinning of Nanofibers and the Charge Injection Method. In *Nanofibers and Nanotechnology in Textiles*; Elsevier: 2007; pp 3−21.
(45) Yarin, A. L.; Zussman, E. Upward Needleless Electrospinning of Multiple Nanofibers. *Polymer* **2004**, *45*, 2977−2980.
(46) Liu, Y.; He, J. H.; Yu, J. Y. Bubble-Electrospinning: A Novel Method for Making Nanofibers. *J. Phys. Conf Ser.* **2008**, *96*, 012001−012001.
(47) Yang, R. R.; He, J. H.; Xu, L.; Yu, J. Y. Bubble-Electrospinning for Fabricating Nanofibers. *Polymer* **2009**, *50*, 5846−5850.
(48) Dosunmu, O. O.; Chase, G. G.; Kataphinan, W.; Reneker, D. H. Electrospinning of Polymer Nanofibres from Multiple Jets on a Porous Tubular Surface. *Nanotechnology* **2006**, *17*, 1123−1127.
(49) Higham, A. K.; Tang, C.; Landry, A. M.; Pridgeon, M. C.; Lee, E. M.; Andrady, A. L.; Khan, S. A. Foam Electrospinning: A Multiple Jet, Needle-Less Process for Nanofiber Production. *AIChE J.* **2014**, *60*, 1355−1364.
(50) Liu, Y. W.; Zhang, L.; Li, H. N.; Yan, S. L.; Yu, J. S.; Weng, J.; Li, X. H. Electrospun Fibrous Mats on Lithographically Micropatterned Collectors to Control Cellular Behaviors. *Langmuir* **2012**, *28*, 17134−17142.
(51) Hotaling, N. A.; Bharti, K.; Kriel, H.; Simon, C. G. Diameterj: A Validated Open Source Nanofiber Diameter Measurement Tool. *Biomaterials* **2015**, *61*, 327−338.
(52) McKee, M. G.; Hunley, M. T.; Layman, J. M.; Long, T. E. Solution Rheological Behavior and Electrospinning of Cationic Polyelectrolytes. *Macromolecules* **2006**, *39*, 575−583.
(53) Sun, Y. Y.; Cui, L. R.; Gong, J.; Zhang, J.; Xiang, Y.; Lu, S. F. Design of a Catalytic Layer with Hierarchical Proton Transport Structure: The Role of Nafion Nanofiber. *ACS Sustainable Chem. Eng.* **2019**, *7*, 2955−2963.
(54) Chen, L.; Hallinan, D. T.; Elabd, Y. A.; Hillmyer, M. A. Highly Selective Polymer Electrolyte Membranes from Reactive Block Polymers. *Macromolecules* **2009**, *42*, 6075−6085.

DOI: 10.1021/acsapm.9b00681
ACS Appl. Polym. Mater. 2019, 1, 2731−2740